

# Unsupervised phase discovery with deep anomaly detection

Korbinian Kottmann,<sup>1</sup> Patrick Huembeli,<sup>1</sup> Maciej Lewenstein,<sup>1,2</sup> and Antonio Acín<sup>1,2</sup>

<sup>1</sup>*ICFO - Institut de Ciències Fòniques, The Barcelona Institute of Science and Technology, Av. Carl Friedrich Gauss 3, 08860 Castelldefels (Barcelona), Spain*

<sup>2</sup>*ICREA, Pg. Lluís Companys 23, 08010 Barcelona, Spain*

We demonstrate how to explore phase diagrams with automated and unsupervised machine learning to find regions of interest for possible new phases. In contrast to supervised learning, where data is classified using predetermined labels, we here perform anomaly detection, where the task is to differentiate a normal data set, composed of one or several classes, from anomalous data. As a paradigmatic example, we explore the phase diagram of the extended Bose Hubbard model in one dimension at exact integer filling and employ deep neural networks to determine the entire phase diagram in a completely unsupervised and automated fashion. As input data for learning, we first use the entanglement spectra and central tensors derived from tensor-networks algorithms for ground-state computation and later we extend our method and use experimentally accessible data such as low-order correlation functions as inputs. Our method allows us to reveal a phase-separated region between supersolid and superfluid parts with unexpected properties, which appears in the system in addition to the standard superfluid, Mott insulator, Haldane-insulating, and density wave phases.

*Introduction* Recent developments in machine learning (ML) have revolutionized the way how we can process and find correlations in complex data. These developments have impacted the physical sciences with a wide variety of applications [1]. Of particular interest is the classification and discovery of phase transitions [2–19]. Recent works concern studies of classical [2, 4], quantum [11, 14, 18] and topological phase transitions [12, 13]. The methods employed range from deep supervised [4, 18] and unsupervised [3, 6] to shallow unsupervised ML algorithms [2, 7, 8, 20]. The input of the ML algorithms can vary from classical spin values [4], local observables [7, 8], correlation functions [14], entanglement spectra [3, 5, 15, 16] to the full state vector [11, 17]. At the same time, the development of the density matrix renormalization algorithm [21, 22] and its reformulation from a quantum information perspective in terms of tensor networks [23, 24] allows one to study large quantum many-body systems approaching the thermodynamic limit.

In this work, we demonstrate how to map out a phase diagram of a quantum many-body system to identify regions of interest for possible new phases using automated and unsupervised machine learning based on anomaly detection [25–27]. This approach is particularly useful when one is confronted with sufficient data from known classes of states and little or no data from unknown classes.

Compared to previous unsupervised attempts in [2, 3, 6–8], this method needs only one or few training iterations and has better generalization properties from employing deep neural networks [30, 31]. This allows for efficient fully automatized phase discovery in the spirit of self-driving laboratories [32], where artificial intelligence augments experimentation platforms to enable fully autonomous experimentation. Intuitively, the method explores the phase diagram until an abrupt change, an anomaly, is detected, singling out the presence of a phase transition. The intuition is similar to the approach intro-

duced in [33], where the authors proposed to detect quantum phase transitions by looking at the overlap between neighbouring ground states in the phase diagram. Here, the machine is used to detect these anomalies. Moreover, as we explain next, it does it from scalable data.

In principle, there are many possible choices as input data for training our method, including the full state vector. To improve scalability and reach large system sizes, we propose to use quantities that arise naturally in the state description and do not require complete state information. For instance, we obtain ground states with tensor networks, from which we use the tensors themselves or the entanglement spectrum (ES) as input data. These quantities arise naturally from the state description without further processing and contain crucial information about the phase, like ES for example [15, 16, 34]. We stress, however, that the choice of preferred quantities to be used for ML may in general vary and depend on the simulation method. In fact, we show that our method also works well with physical data accessible in experiments such as low-order correlation functions.

As a benchmark, we apply our method to the extended Bose Hubbard model in one dimension at exact integer filling. Its phase diagram is very rich and therefore provides a very good test to showcase our method. We are able to determine the entire phase diagram in a completely unsupervised and automated fashion. Importantly, our results point out the existence of a supersolid state that appears in the system in addition to the standard superfluid, Mott insulator, Haldane-insulating, and density-wave phases.

*Anomaly Detection Method* In this work, we apply deep neural network autoencoders for anomaly detection [27]. An autoencoder (AE) is a type of neural network that consists of two parts. The encoder part takes the  $D$ -dimensional input data point  $x$  and maps it to a  $k$  dimensional latent variable  $z$  (typically  $k < D$ ) via a parametrized function  $z = f_\phi(x)$ . The decoder part takes

the latent variable  $z$  and maps it back to  $\bar{x} = g_\theta(z)$ . The parameters  $\phi$  and  $\theta$  are trained via the minimization of a loss function  $L(x, \bar{x})$  that measures the dissimilarity of the input  $x$  and the output  $\bar{x}$ . The aim of the training is that the input is identical to the output for the whole training data set  $\{x\}$ . Heuristically, we find that the *mean-square error*  $L(x, \bar{x}) = \sum_v |x_v - \bar{x}_v|^2 / D$  suffices for this endeavour and provides good results.

The idea of this anomaly detection scheme is that for each state  $|\psi\rangle$  we take corresponding data  $x$ , such as for instance its ES or low order correlation functions. That data has characteristic features that the AE learns to encode into the latent variable  $z$  at the bottleneck [35], from which it is ideally able to reconstruct the original input. The loss  $L$  directly indicates the success of this endeavour, which we improve by employing symmetric shortcut connections (SSC, see fig. 1), inspired from [36, 37] to typical losses  $< 5\%$ . Now, the intuition is that, when confronted with data from unknown phases, the AE is unable to encode and decode  $x$ . This leads to a higher loss, from which we deduce that the states do not belong to the same phase as the ones used to train the AE.

Deep learning architectures are known to generalize well [30, 31], such that it suffices to train in a small region of the parameter space. Compared to known supervised deep learning methods this anomaly detection scheme does not rely on labeled data. We choose training data from one or several regions of the phase diagram, and ask how the loss of a test data point from any region of the phase diagram compares to the loss of these training points. As we show later, this can be performed with no a priori knowledge and in a completely unsupervised manner. The computationally most expensive step is the training and with our method it has to be performed only once to map the whole phase diagram, as opposed to multiple trainings like in [3, 6]. Furthermore, it does not require a full description of the physical states in contrast to [33], where full contraction is necessary. Thus, for higher dimensional systems, [33] is infeasible as contraction is known to be generally inefficient for 2d tensor network states (commonly referred to as PEPS, see [24]).

The specific architecture in use consists of two 1d-convolutional encoding and decoding layers with SSCs (Figure 1), implemented in TensorFlow [38]. To ensure the reproducibility of our results, we made the source code available under an open source license [39].

*Simulation Method* We calculate the ground states by means of the Density Matrix Renormalization Group algorithm (DMRG) in terms of Tensor Networks, i.e. Matrix Product States (MPS) [23, 24]. A general multipartite state of  $L$  parties with local dimension  $d$   $|\Psi\rangle = \sum_{\sigma} c_{\sigma} |\sigma\rangle$ , where  $\sigma = \sigma_1 \dots \sigma_L$  is the vector of local indices  $\sigma_i = 1, \dots, d$ , can always be decomposed into products of tensors with the aid of the singular value decomposition. We use the convention of Vidal [40], and write our ground state in the MPS form

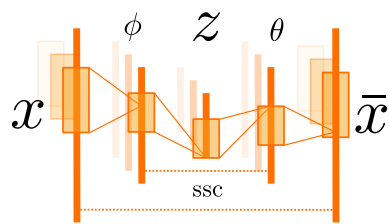


FIG. 1. Schematic one-dimensional convolutional neural network autoencoder with symmetric shortcut connections (SSC) that connect latent layers of the same dimension directly via addition, thereby improving the model performance [36, 37]. Shaded boxes in the background indicate schematically the convolutional nature of the layers. We illustrate how the input data  $x$  gets encoded into the lower dimensional latent vector  $z$  and decoded again to  $\bar{x}$ .

$$|\Psi\rangle = \sum_{\sigma} \Gamma^{\sigma_1} \Lambda^{[1]} \dots \Lambda^{[i-1]} \Gamma^{\sigma_i} \Lambda^{[i]} \dots \Lambda^{[L-1]} \Gamma^{\sigma_L} |\sigma_1 \dots \sigma_i \dots \sigma_L\rangle. \quad (1)$$

At site  $i$ ,  $\{\Gamma^{\sigma_i}\}$  is a set of  $d$  matrices and  $\Lambda^{[i]}$  the diagonal singular value matrix of a bipartition of the chain between site  $i$  and  $i+1$ , i.e. the Schmidt values (see [23]). One then approximates the exact ground state by keeping only the  $\chi_{\max}$  largest Schmidt values for each partition, where  $\chi_{\max}$  is known as the bond dimension. This is the best approximation of the full state in terms of the Frobenius norm and enables us to handle big system sizes. Eq. (1) corresponds to finite length and open boundary conditions. Here, we use the version formulated in the thermodynamic limit for infinite MPS (iMPS) [41–43]. In this case, instead of a finite chain, we are effectively operating in the thermodynamic limit and have a finite but repeating unit cell of length  $L_{\infty}$ .

We use the Schmidt values  $\Lambda^{[i]}$  as our input data  $x$  to explore the phase diagram and ambiguously refer to it as ES. Our numerical results support the functionality of using this anomaly detection scheme with ES as we get near-constant losses for states of the training region and significantly higher losses for unknown phases. The method generalizes well with similar losses for states inside and outside the training region. As we will see below, the method works even well for transitions of Berezinskii-Kosterlitz-Thouless (BKT) type, where the exact transition point is hard to determine in terms of observable correlation functions, and symmetry protected topological (i.e. global) order.

*Hamiltonian* We test our method on the extended Bose-Hubbard Model

$$H = -t \sum_i \left( b_i^\dagger b_{i+1} + b_{i+1}^\dagger b_i \right) + \frac{U}{2} \sum_i n_i (n_i - 1) + V \sum_i n_i n_{i+1}, \quad (2)$$

with nearest neighbour interaction on a one dimensional chain. It serves as a highly non-trivial test ground with its rich phase diagram that, beside a critical superfluid and two insulating phases, admits a symmetry protected topologically ordered phase at commensurate fillings [34, 44–52]. Here,  $n_i = b_i^\dagger b_i$  is the number operator for Bosons defined by  $[b_i, b_j^\dagger] = \delta_{ij}$ . Typically, we are interested in varying the on-site interaction  $U$  and nearest-neighbour interaction  $V$  and fix the hopping term  $t = 1$ . We explicitly enforce filling  $\bar{n} := \sum_i \langle n_i \rangle / L_\infty = 1$  by employing  $U(1)$  symmetric tensors [53], which we implement using the open source library TeNPy [54] (easily readable code accessible in [39]).

One way to physically classify these phases is to look at the correlators

$$C_{\text{SF}}(i, j) = \langle b_i^\dagger b_j \rangle \quad (3)$$

$$C_{\text{DW}}(i, j) = \langle \delta n_i (-1)^{|i-j|} \delta n_j \rangle \quad (4)$$

$$C_{\text{HI}}(i, j) = \langle \delta n_i \exp \left( -i\pi \sum_{i \leq l \leq j-1} \delta n_l \right) \delta n_j \rangle \quad (5)$$

with  $\delta n_i = n_i - \bar{n}$ .  $C_{\text{SF}}$  discriminates the Mott-insulating (MI) phase and the superfluid (SF) phase, where it decays exponentially and with a power-law, respectively. The correlators for density-wave (DW) and Haldane-insulating (HI) phases decay to a constant value in the respective phases. More details about the characterization of the system can be found in [44] and the supplementary material (SM). The non-local string term in eq. (5) is characteristic of topological order, where the translational symmetry remains protected with a transition in the Luttinger liquid universality class from MI and gets broken with a transition in the Ising universality class to DW [52]. We visualize the phase diagram by computing  $O_\bullet = \sum_{i,j} C_\bullet(i, j) / L_\infty^2$  in fig. 2 in the thermodynamic limit for a repeating unit cell of  $L_\infty = 64$  sites with a maximum bond dimension  $\chi_{\text{max}} = 100$  and assuming a maximum occupation number  $n_{\text{max}} = 3$ , which results in a local dimension  $d = n_{\text{max}} + 1 = 4$ . We use data from these states, obtained with these parameters throughout the rest of the following analysis.

*Numerical Results* Assuming no a priori knowledge, we start by training with data points at the origin of the parameter space  $(U, V) \in [0, 1.3]^2$ , which in our case accounts to training in SF. By testing with data points from the whole phase diagram we can clearly see the boundaries to all other phases from SF in fig. 3. The BKT transition between SF and MI is matched by an

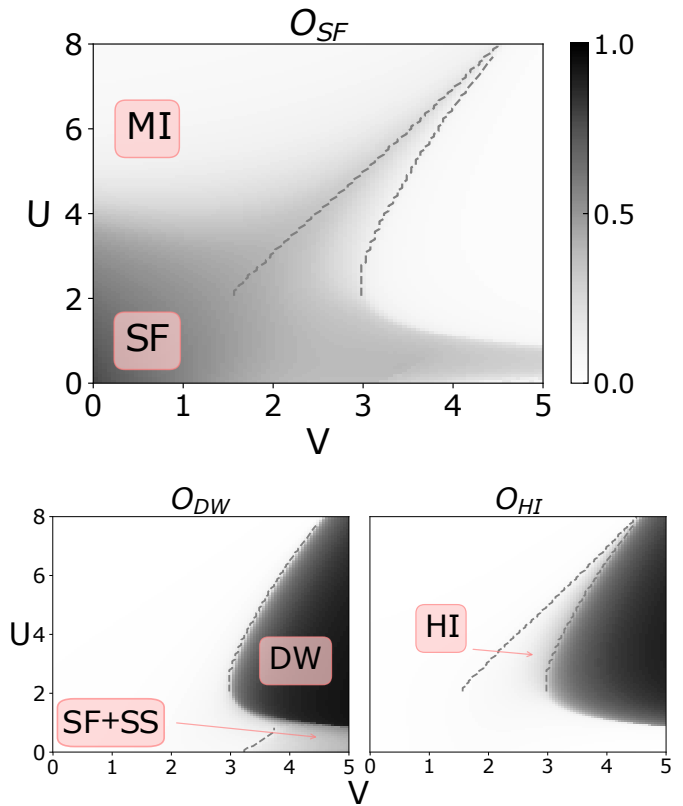


FIG. 2. Extended BH phase diagram with five distinct phases obtained by the correlators eqs. (3) to (5). MI: Mott Insulator, SF: Super Fluid, SS: Super Solid, DW: Density Wave, HI: Haldane Insulator. The dashed lines indicate the transition points observed from diverging correlation lengths between MI-HI-DW and non-zero  $S$  in eq. (6) between SF and SF+SS.

abrupt rise in loss (fig. 3, inset a)). In this particular case, we can already determine the different phases inside the anomalous region due to their different loss levels and the appearance of two valleys at the phase boundaries between MI, HI and SF (fig. 3, inset b)). Physically, we can explain these valleys by the criticality of these Luttinger and Ising type transitions, which lead to a slowly decaying ES at the boundary, just like in the critical SF phase.

It is not necessarily always the case that one can differentiate the different phases inside the high-loss anomalous region. Thus, as a systematic approach, we propose picking homogeneous and high contrast anomalous regions after the initial training. Here, we already mapped out the whole phase diagram after the first training iteration, so we leave a possible continuation in  $(U, V) \in [4, 4.8] \times [2, 4]$  to the SM. This method is not tailored to ES as input data. To show this, we use on one hand tensors from the MPS as input data in the SM. On the other hand we use experimentally accessible correlators. In fig. 4, instead of unprocessed data from simulation,

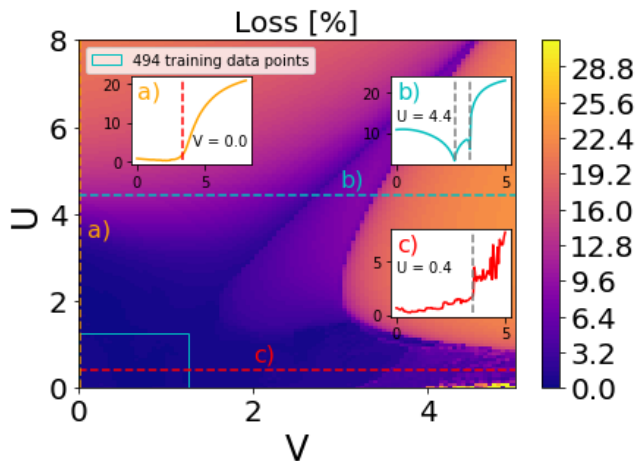


FIG. 3. 2D loss map of the AE after training near the parameter space origin (blue square frame). The insets a), b) and c) show the loss along the dashed lines. Vertical green dashed line in inset a) indicates critical  $U_c = 3.33$  [46]. Vertical grey dashed lines in inset b) and c) are the transitions from fig. 2. The phase boundaries are determined by a rise in loss (inset a) and c)). The anomalous regions are already well-separated by decreasing losses because of the critical behaviour at the phase boundaries (inset b)), which share similarities with the critical SF phase. Higher loss indicates that this region is more different from the training region in the blue square, lower loss indicates similarity.

we calculate  $\{C_{SF}(i, j)\}_{i, j=1}^{64}$  and train in MI and SF simultaneously. We interpret rows as color channels for 1d convolution. Because  $C_{SF}$  does not contain any information about the topological order in HI, the method does not recognize this region as we would expect (fig. 4, inset a)). Overall, the boundaries match perfectly with a sharp increase onto a plateau at the transition points. This opens the possibility to use physical observables from experiment with the caveat of requiring physical knowledge a priori.

By close inspection of figs. 3 and 4, we see a region with noticeable contrast for small  $U$  and large  $V$ , indicating the presence of a separate phase. This is interesting because, initially, we did not expect to find a fifth phase in the diagram. Upon further physical investigation, we find a phase-separated state between SF and supersolid (SF + SS). Supersolidity in this model has been studied in previous literature for incommensurate fillings [19, 45–47] and was claimed to be found for filling 1 in [34] without further discussion. The phase separation that we find here is new and has not been studied before to the best of our knowledge. In order to physically show the transition, we compute the Fourier transform of the local density  $\tilde{n}(k) = \sum_j \langle n_j \rangle e^{-ikj} / L_\infty$  and detect long-range solid order by looking at

$$S := \max_{k \neq 0} |\tilde{n}(k)|^2 \quad (6)$$

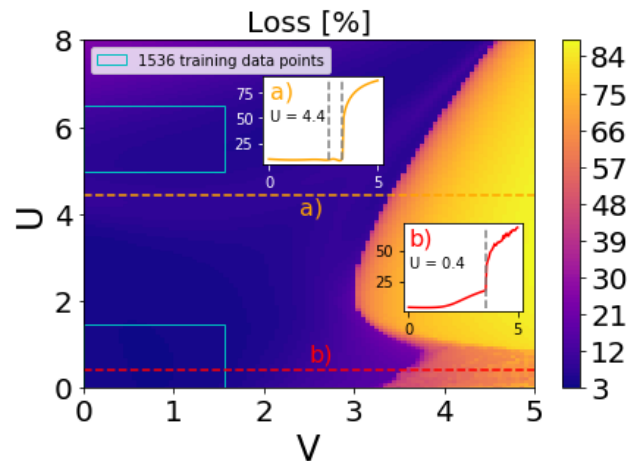


FIG. 4. 2D loss map of the AE after training in the two blue square frames in the SF and the MI phase. The insets a) and b) show the loss along the dashed lines. Instead of the ES, we use the physically accessible correlator  $C_{SF}$  as input data. The HI is not recognized as this correlator does not contain information about the topological order of this phase.

in fig. 5 [55]. Additionally, we find non-zero  $O_{DW}$  and  $O_{SF}$ , showing both superfluid and crystalline behavior. For higher numerical accuracy and better illustration of the correlator decay, we compute a larger state for  $L_\infty = 200$ ,  $d = 6$  and  $\chi_{\max} = 500$  at  $(U, V) = (0.5, 4)$  and see both crystalline and superfluid regions in the density profile  $\langle n_j \rangle$ , fig. 5 inset a). To confirm supersolidity of the crystalline part we show that  $C_{SF}$  decays with a power-law in that region, see fig. 5 inset b).

This phase separation occurs as the system becomes mechanically unstable. We can see this as the second derivative of the ground state energy per site  $\mathcal{E} = E/L$  with respect to the filling  $f$  vanishes. We perform finite size scaling with open boundary conditions to show this in fig. 6. There, we target equidistant discrete fillings  $f_i = N_i/L$  for  $N_i \in [0.8L, 1.1L]$  and compute the finite difference derivative  $d^2\mathcal{E}/df^2 = (\mathcal{E}(f_{i-1}) - 2\mathcal{E}(f_i) + \mathcal{E}(f_{i+1})) / (f_i - f_{i-1})^2$ . The detection of this new phase demonstrates the power of our approach and we leave further physical investigation to future work.

*Conclusion* We have shown an unsupervised method to map out the phase diagram of a complex quantum many-body system that could possibly be performed fully data driven and without physical a priori knowledge such as the construction of an order parameter. By using tensor networks we can reliably compute ground states of many-body systems in the thermodynamic limit and at the same time extract the desired data without further processing. Entanglement spectra and central tensors serve as natural quantities in this context, but the method also proved successful for physical observables like  $\langle b_i^\dagger b_j \rangle$  correlators. Hence, this method can be applied

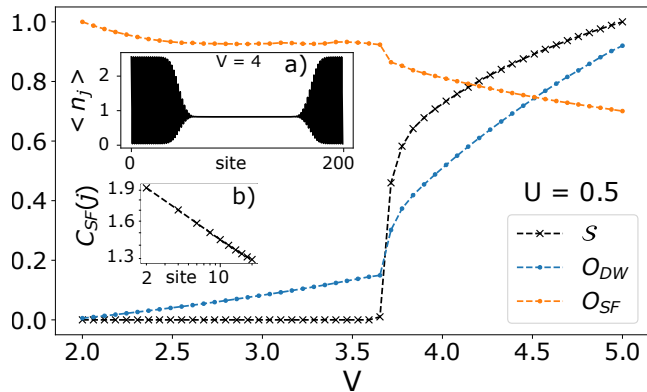


FIG. 5. Transition from SF to phase separated SF + SS at fixed  $U=0.5$ . The solid long-range order emerges while SF correlations sustain. Inset a) shows the phase separation in the density  $\langle n_j \rangle$  for a state at  $(U, V) = (0.5, 4)$  with  $L_\infty = 200$ ,  $d = 6$  and  $\chi_{\max} = 500$ . Inset b) shows the power-law decay of  $C_{SF}(0, j)$  in the solid part via doubly logarithmic plot of every second value, confirming supersolidity.

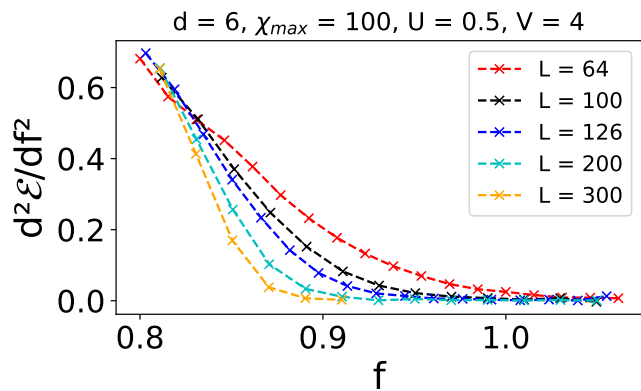


FIG. 6. Finite size scaling of the vanishing second derivative of the ground state energy per site  $\mathcal{E}$  with respect to the filling  $f$ . This shows that the system becomes mechanically unstable, leading to phase separation as depicted in fig. 5 for  $f = 1$ .

in both purely computational platforms like self-driving laboratories as well as experimental setups.

## ACKNOWLEDGMENTS

We thank E. Tirrito, D. Gonzalez-Cuadra, A. Dauphin, G. Astrakharchik and P. Massignan for helpful insights and discussions. This project has received funding from the European Union’s Horizon 2020 research and innovation programme under the Marie Skłodowska-Curie grant agreement No 665884 (P.H.) and 713729 (K.K.). We acknowledge the Spanish Ministry MINECO (National Plan 15 Grant: FISICATEAMO No. FIS2016-79508-P, TRANQI, SEVERO OCHOA No. SEV-2015-0522), European Social Fund, Fundacio Cellex and Mir-Puig, Generalitat de Catalunya (AGAUR SGR 1341, SGR1381, QuantumCAT and CERCA/Program), ERC AdGs NOQIA and CERQUTE, the AXA Chair in Quantum Information Science and the National Science Centre, Poland-Symfonia Grant No.2016/20/W/ST4/00314.

[1] Giuseppe Carleo, Ignacio Cirac, Kyle Cranmer, Laurent Daudet, Maria Schuld, Naftali Tishby, Leslie Vogt-Maranto, and Lenka Zdeborová, “Machine learning and the physical sciences,” (2019), [10.1103/RevModPhys.91.045002](https://arxiv.org/abs/10.1103/RevModPhys.91.045002), [arXiv:1903.10563](https://arxiv.org/abs/1903.10563).

[2] Lei Wang, “Discovering phase transitions with unsupervised learning,” *Physical Review B* **94**, 195105 (2016), [arXiv:1606.00318](https://arxiv.org/abs/1606.00318).

[3] Evert P.L. van Nieuwenburg, Ye-Hua Liu, and Sebastian D. Huber, “Learning phase transitions by confusion,” *Nature Physics*, 4037 (2017), [arXiv:1610.02048](https://arxiv.org/abs/1610.02048).

[4] Juan Carrasquilla and Roger G. Melko, “Machine learning phases of matter,” *Nature Physics* **13**, 431–434 (2017), [arXiv:1605.01735](https://arxiv.org/abs/1605.01735).

[5] Frank Schindler, Nicolas Regnault, and Titus Neupert, “Probing many-body localization with neural networks,” *Physical Review B* **95**, 245134 (2017), [arXiv:1704.01578](https://arxiv.org/abs/1704.01578).

[6] Ye-Hua Liu and Evert P. L. van Nieuwenburg, “Self-learning phase boundaries by active contours,” (2017), [arXiv:1706.08111](https://arxiv.org/abs/1706.08111).

[7] Sebastian Johann Wetzels, “Unsupervised learning of phase transitions: from principal component analysis to variational autoencoders,” *Physical Review E* **96**, 022140

- (2017), [arXiv:1703.02435](#).
- [8] Kelvin Ch'ng, Nick Vazquez, and Ehsan Khatami, “Unsupervised machine learning account of magnetic transitions in the hubbard model,” *Physical Review E* **97**, 013306 (2018), [arXiv:1708.03350](#).
- [9] Maciej Koch-Janusz and Zohar Ringel, “Mutual information, neural networks and the renormalization group,” (2017), [arXiv:1704.06279](#).
- [10] Patrick Huembeli, Alexandre Dauphin, and Peter Wittek, “Identifying quantum phase transitions with adversarial neural networks,” *Physical Review B* **97**, 134109 (2018), [arXiv:1710.08382](#).
- [11] Patrick Huembeli, Alexandre Dauphin, Peter Wittek, and Christian Gogolin, “Automated discovery of characteristic features of phase transitions in many-body localization,” *Physical Review B* **99**, 104106 (2019), [arXiv:1806.00419](#).
- [12] Dong-Ling Deng, Xiaopeng Li, and S. Das Sarma, “Exact machine learning topological states,” [arXiv:1609.09060](#) (2016).
- [13] Pengfei Zhang, Huitao Shen, and Hui Zhai, “Machine learning topological invariants with neural networks,” (2017), [arXiv:1708.09401](#).
- [14] Peter Broecker, Juan Carrasquilla, Roger G. Melko, and Simon Trebst, “Machine learning quantum phases of matter beyond the fermion sign problem,” *Scientific Reports* **8**, 8823 (2017), [arXiv:1608.07848](#).
- [15] Yuan-Hong Tsai, Meng-Jer Yu, Yu-Hao Hsu, and Ming-Chiang Chung, “Deep learning of topological phase transitions from entanglement aspects,” (2019), [arXiv:1909.04784](#).
- [16] Kazuya Shinjo, Kakeru Sasaki, Satoru Hase, Shigetoshi Sota, Satoshi Ejima, Seiji Yunoki, and Takami Tohyama, “Machine Learning Phase Diagram in the Half-filled One-dimensional Extended Hubbard Model,” (2019), [10.7566/JPSJ.88.065001](#), [arXiv:1904.06032](#).
- [17] Hugo Théveniaut and Fabien Alet, “Neural network setups for a precise detection of the many-body localization transition: finite-size scaling and limitations,” *Physical Review B* **100**, 224202 (2019), [arXiv:1904.13165](#).
- [18] Xiao-Yu Dong, Frank Pollmann, and Xue-Feng Zhang, “Machine learning of quantum phase transitions,” (2018), [10.1103/PhysRevB.99.121104](#), [arXiv:1806.00829](#).
- [19] Keima Kawaki, Yoshihito Kuno, and Ikuo Ichinose, “Phase diagrams of the extended bose-hubbard model in one dimension by monte-carlo simulation with the help of a stochastic-series expansion,” *Phys. Rev. B* **95**, 195101 (2017), [arXiv:1701.00613](#).
- [20] Zohar Nussinov, Peter Ronhovde, Dandan Hu, S Chakrabarty, Bo Sun, Nicholas A Mauro, and Kisor K Sahu, “Inference of hidden structures in complex physical systems by multi-scale clustering,” in *Information Science for Materials Discovery and Design* (Springer, 2016) pp. 115–138.
- [21] Steven R. White, “Density matrix formulation for quantum renormalization groups,” *Physical Review Letters* **69**, 2863–2866 (1992).
- [22] Steven R. White, “Density-matrix algorithms for quantum renormalization groups,” *Physical Review B* **48**, 10345–10356 (1993).
- [23] Ulrich Schollwöck, “The density-matrix renormalization group in the age of matrix product states,” *Annals of Physics* **326**, 96–192 (2011).
- [24] Roman Orus, “A Practical Introduction to Tensor Networks: Matrix Product States and Projected Entangled Pair States,” (2013), [10.1016/j.aop.2014.06.013](#), [arXiv:1306.2164](#).
- [25] Raghavendra Chalapathy and Sanjay Chawla, “Deep learning for anomaly detection: A survey,” *arXiv preprint arXiv:1901.03407* (2019), [arXiv:1901.03407](#).
- [26] Donghwoon Kwon, Hyunjoo Kim, Jinho Kim, Sang C Suh, Ikkyun Kim, and Kuinam J Kim, “A survey of deep learning-based network anomaly detection,” *Cluster Computing*, 1–13 (2017).
- [27] Andrea Borghesi, Andrea Bartolini, Michele Lombardi, Michela Milano, and Luca Benini, “Anomaly detection using autoencoders in high performance computing systems,” in *Proceedings of the AAAI Conference on Artificial Intelligence*, Vol. 33 (2019) pp. 9428–9433, [arXiv:1811.05269](#).
- [28] Utkarsh Porwal and Smruthi Mukund, “Credit card fraud detection in e-commerce: An outlier detection approach,” (2018), [arXiv:1811.02196](#).
- [29] Philipp Seeböck, Sebastian Waldstein, Sophie Klimscha, Bianca S Gerendas, René Donner, Thomas Schlegl, Ursula Schmidt-Erfurth, and Georg Langs, “Identifying and categorizing anomalies in retinal imaging data,” (2016), [arXiv:1612.00686](#).
- [30] Kenji Kawaguchi, Leslie Pack Kaelbling, and Yoshua Bengio, “Generalization in deep learning,” (2017), [arXiv:1710.05468](#).
- [31] Guillermo Valle-Pérez, Chico Q Camargo, and Ard A Louis, “Deep learning generalizes because the parameter-function map is biased towards simple functions,” (2018), [arXiv:1805.08522](#).
- [32] Florian Häse, Loïc M. Roch, and Alán Aspuru-Guzik, “Next-Generation Experimentation with Self-Driving Laboratories,” *Trends in Chemistry* **1**, 282–291 (2019).
- [33] P. Zanardi, M. Cozzini, and P. Giorda, “Ground state fidelity and quantum phase transitions in free Fermi systems,” (2006), [10.1088/1742-5468/2007/02/L02002](#), [arXiv:0606130 \[quant-ph\]](#).
- [34] Xiaolong Deng and Luis Santos, “Entanglement spectrum of one-dimensional extended Bose-Hubbard models,” (2011), [10.1103/PhysRevB.84.085138](#), [arXiv:1104.5157](#).
- [35] Raban Iten, Tony Metger, Henrik Wilming, Lúcia del Rio, and Renato Renner, “Discovering Physical Concepts with Neural Networks,” *Physical Review Letters* **124**, 010508 (2020), [1807.10300](#).
- [36] Jianfeng Dong, Xiao-Jiao Mao, Chunhua Shen, and Yu-Bin Yang, “Learning Deep Representations Using Convolutional Auto-encoders with Symmetric Skip Connections,” (2016), [arXiv:1611.09119](#).
- [37] Jianfeng Dong, Xiao-Jiao Mao, Chunhua Shen, and Yu-Bin Yang, “Unsupervised feature learning with symmetrically connected convolutional denoising auto-encoders,” *CoRR abs/1611.09119* (2016), [arXiv:1611.09119](#).
- [38] Martín Abadi, Ashish Agarwal, Paul Barham, Eugene Brevdo, Zhifeng Chen, Craig Citro, Greg S. Corrado, Andy Davis, Jeffrey Dean, Matthieu Devin, Sanjay Ghemawat, Ian Goodfellow, Andrew Harp, Geoffrey Irving, Michael Isard, Yangqing Jia, Rafal Jozefowicz, Lukasz Kaiser, Manjunath Kudlur, Josh Levenberg, Dandelion Mané, Rajat Monga, Sherry Moore, Derek Murray, Chris Olah, Mike Schuster, Jonathon Shlens, Benoit Steiner, Ilya Sutskever, Kunal Talwar, Paul Tucker,

- Vincent Vanhoucke, Vijay Vasudevan, Fernanda Viégas, Oriol Vinyals, Pete Warden, Martin Wattenberg, Martin Wicke, Yuan Yu, and Xiaoqiang Zheng, “TensorFlow: Large-scale machine learning on heterogeneous systems,” (2015), software available from tensorflow.org.
- [39] Korbinian Kottmann and Patrick Huembeli, “Unsupervised phase discovery with deep anomaly detection,” <https://github.com/Qottmann/phase-discovery-anomaly-detection/> (2020).
- [40] Guifre Vidal, “Efficient classical simulation of slightly entangled quantum computations,” (2003), 10.1103/PhysRevLett.91.147902, arXiv:0301063 [quant-ph].
- [41] G. Vidal, “Classical simulation of infinite-size quantum lattice systems in one spatial dimension,” (2006), 10.1103/PhysRevLett.98.070201, arXiv:0605597 [cond-mat].
- [42] Ian P. McCulloch, “From density-matrix renormalization group to matrix product states,” (2007), 10.1088/1742-5468/2007/10/P10014, arXiv:0701428 [cond-mat].
- [43] R. Orús and G. Vidal, “Infinite time-evolving block decimation algorithm beyond unitary evolution,” *Physical Review B* **78**, 155117 (2008).
- [44] Davide Rossini and Rosario Fazio, “Phase diagram of the extended Bose Hubbard model,” (2012), 10.1088/1367-2630/14/6/065012, arXiv:1204.5964.
- [45] Till D. Kuehner and H. Monien, “Phases of the one-dimensional Bose-Hubbard model,” (1997), 10.1103/PhysRevB.58.R14741, arXiv:9712307 [cond-mat].
- [46] Till D. Kuehner, Steven R. White, and H. Monien, “The one-dimensional Bose-Hubbard Model with nearest-neighbor interaction,” (1999), 10.1103/PhysRevB.61.12474, arXiv:9906019 [cond-mat].
- [47] Tapan Mishra, Ramesh V. Pai, S. Ramanan, Meetu Sethi Luthra, and B. P. Das, “Supersolid and solitonic phases in one-dimensional Extended Bose-Hubbard model,” (2009), 10.1103/PhysRevA.80.043614, arXiv:0907.1258.
- [48] Laura Urba, Emil Lundh, and Anders Rosengren, “One-dimensional extended Bose-Hubbard model with a confining potential: A DMRG analysis,” *Journal of Physics B: Atomic, Molecular and Optical Physics* **39**, 5187–5198 (2006), arXiv:0607722 [cond-mat].
- [49] Satoshi Ejima, Florian Lange, and Holger Fehske, “Spectral and Entanglement Properties of the Bosonic Haldane Insulator,” (2014), 10.1103/PhysRevLett.113.020401, arXiv:1407.2852.
- [50] M. A. Cazalilla, R. Citro, T. Giamarchi, E. Orignac, and M. Rigol, “One dimensional Bosons: From Condensed Matter Systems to Ultracold Gases,” (2011), 10.1103/RevModPhys.83.1405, arXiv:1101.5337.
- [51] G. G. Batrouni, F. Hebert, and R. T. Scalettar, “Supersolid phases in the one dimensional extended soft core Bosonic Hubbard model,” (2006), 10.1103/PhysRevLett.97.087209, arXiv:0605218 [cond-mat].
- [52] Erez Berg, Emanuele G. Dalla Torre, Thierry Giamarchi, and Ehud Altman, “Rise and fall of hidden string order of lattice bosons,” (2008), 10.1103/PhysRevB.77.245119, arXiv:0803.2851.
- [53] Pietro Silvi, Ferdinand Tschirsich, Matthias Gerster, Johannes Jünemann, Daniel Jaschke, Matteo Rizzi, and Simone Montangero, “The Tensor Networks Anthology: Simulation techniques for many-body quantum lattice systems,” *SciPost Phys. Lect. Notes*, **8** (2019), arXiv:1710.03733.
- [54] Johannes Hauschild and Frank Pollmann, “Efficient numerical simulations with Tensor Networks: Tensor Network Python (TeNPy),” *SciPost Phys. Lect. Notes*, **5** (2018), code available from <https://github.com/tenpy/tenpy>, arXiv:1805.00055.
- [55] Yung-Chung Chen and Min-Fong Yang, “Two supersolid phases in hard-core extended Bose-Hubbard model,” (2017), 10.1088/2399-6528/aa8bfb, arXiv:1703.05866.
- [56] AF Andreev and IM Lifshits, “Quantum theory of defects in crystals,” *Zhur Eksper Teoret Fiziki* **56**, 2057–2068 (1969).
- [57] G. V. Chester, “Speculations on bose-einstein condensation and quantum crystals,” *Phys. Rev. A* **2**, 256–258 (1970).
- [58] Grigory E. Astrakharchik, Konstantin V. Krutitsky, Maciej Lewenstein, Ferran Mazzanti, and Jordi Boronat, “Optical lattices as a tool to study defect-induced superfluidity,” (2016), 10.1103/PhysRevA.96.033606, arXiv:1612.07690.